Received: 20 November 2020 | Revised: 8 January 2021 | Accepted: 19 January 2021

DOI: 10.1111/gtc.12830

ORIGINAL ARTICLE

Genes to Cells WILEY

The role of eutherian-specific *RTL1* in the nervous system and its implications for the Kagami-Ogata and Temple syndromes

Moe Kitazawa[1] | **Akito Sutani**[1,2] | **Tomoko Kaneko-Ishino**[3] | **Fumitoshi Ishino**[1]

[1]Department of Epigenetics, Medical Research Institute, Tokyo Medical and Dental University (TMDU), Tokyo, Japan

[2]Department of Pediatrics and Developmental Biology, Tokyo Medical and Dental University (TMDU), Tokyo, Japan

[3]Department of Nursing, School of Medicine, Tokai University, Kanagawa, Japan

Correspondence
Tomoko Kaneko-Ishino, Department of Nursing, School of Medicine, Tokai University, Kanagawa, Japan.
Email: tkanekoi@is.icc.tokai-u.ac.jp

Fumitoshi Ishino, Department of Epigenetics, Medical Research Institute, Tokyo Medical and Dental University (TMDU), Tokyo, Japan.
Email: fishino.epgn@mri.tmd.ac.jp

Funding information
This work was supported by the funding program for Grants-in-Aid for Scientific Research (A) (16H02478 and 19H00978) from Japan Society for the Promotion of Science (JSPS) to F.I. and T.K.-I., Grants-in-Aid for Research Activity Start-up to M.K. and Joint Usage/Research Program of Medical Research Institute Tokyo Medical and Dental University (TMDU) grants to T.K.-I. and F.I.

Communicated by: Tetsuya Taga

Abstract

RTL1 (also termed paternal expressed 11 (*PEG11*)) is considered the major imprinted gene responsible for the placental and fetal/neonatal muscle defects that occur in the Kagami–Ogata and Temple syndromes (KOS14 and TS14, respectively). However, it remains elusive whether *RTL1* is also involved in their neurological symptoms, such as behavioral and developmental delay/intellectual disability, feeding difficulties, motor delay, and delayed speech. Here, we demonstrate that the mouse RTL1 protein is widely expressed in the central nervous system (CNS), including the limbic system. Importantly, two disease model mice with over- and under-expression of *Rtl1* exhibited reduced locomotor activity, increased anxiety, and impaired amygdala-dependent cued fear, demonstrating that *Rtl1* also plays an important role in the CNS. These results indicate that the KOS14 and TS14 are neuromuscular as well as neuropsychiatric diseases caused by irregular CNS *RTL1* expression, presumably leading to impaired innervation of motor neurons to skeletal muscles as well as malfunction of the hippocampus-amygdala complex. It is of considerable interest that eutherian-specific *RTL1* is expressed in mammalian- and eutherian-specific brain structures, that is, the corticospinal tract and corpus callosum, respectively, suggesting that *RTL1* might have contributed to the acquisition of both these structures themselves and fine motor skill in eutherian brain evolution.

KEYWORDS

a eutherian-specific acquired gene, brain evolution, corpus callosum, corticospinal tract, cranial and spinal nerves, KOS14 and TS14, neuromuscular disease, neuropsychiatric disease, *RTL1/PEG11*

1 | INTRODUCTION

The Kagami–Ogata and Temple syndromes (KOS14 and TS14) are genomic imprinting diseases caused by aberrant regulation of the imprinted region on human chromosome 14, such as paternal and maternal duplication, maternal and paternal deletion as well as gain and loss of DNA methylation at the intergenic differentially methylated region (IG-DMR), respectively (Kotzot, 2004; Kagami et al., 2005, 2008; Ioannides et al., 2014; Ogata & Kagami, 2016). KOS14

Moe Kitazawa and Akito Sutani are equally contributed.

patients exhibit neonatal lethality, presumably due to respiratory problems associated with a small bell-shaped thorax, abdominal wall defects, such as omphalocele and diastasis recti, placentomegaly, polyhydramnios, developmental delay, and/or intellectual disability and feeding disorders (Kagami et al., 2005 and Kagami et al., 2015) (Appendix S1: Table S1). TS14 patients exhibit severe pre- and postnatal growth retardation, hypotonia, early onset of puberty, motor delay, feeding difficulties, and mild intellectual disability (Ioannides et al., 2014; Kagami et al., 2017) (Appendix S1: Table S2).

We previously demonstrated by means of mouse disease models that over-expression and deficiency of retrotransposon Gag like 1 (*Rtl1*, also called as *Peg11*) are responsible for placental abnormalities (Sekita et al., 2008; Kagami et al., 2008; Kitazawa et al., 2017) as well as fetal/neonatal muscle defects, especially in the respiratory-related intercostal, abdominal, and diaphragm muscles in these syndromes (Kitazawa et al., 2020). However, the genetic cause(s) of their neurological defects, such as feeding difficulties, motor delay, and developmental delay/intellectual disability, remains elusive.

In this work, we investigated whether *RTL1* is involved in these neurological symptoms in KOS14 and TS14 by conducting analyses of its expression in the nervous system as well as behavioral analyses of two mouse models with over- and under-expression of *Rtl1*. Although brain *RTL1/Rtl1* expression was present at a low level in humans and mice, we clearly detected a mouse RTL1 protein in the central nervous system (CNS). Two mouse models with over- and under-expression of *Rtl1* exhibited impaired locomotive and cognitive activities. We will discuss the neuromuscular and neuropsychiatric aspects of KOS14 and TS14 caused by irregular RTL1 expression in the brain based on these results.

Interestingly, RTL1 expression was observed in the corticospinal tract responsible for fine voluntary skilled muscle movement of limbs, and the corpus callosum responsible for interhemisphere communication. Evolutionarily, the former is unique to mammals (Aboitiz & Montiel, 2003; Mihrshahi, 2006): the nerve bundles originate in the cerebral cortex layer V and pass through the internal capsule and cerebral peduncles of the midbrain, pons and medulla until they reach the spinal cord (Patestas & Gartner, 2016). The corpus callosum is unique to eutherians (Mihrshahi, 2006; Suárez et al., 2014) and is comprised of nerve fibers coming mainly from cerebral cortex layers II and III (the upper layers) and partially from layers V and VI (the lower layers) (Fame et al., 2011). In placental mammals, the commissure systems originate in the same plate in the embryonic brain and the anterior commissure forms first, followed by the hippocampal commissure and then the corpus callosum (Mihrshahi, 2006). Therefore, it is suggested that the evolution of the corpus callosum involved a rerouting of dorsal cortical axons (Suárez et al., 2014). We confirmed that RTL1 is expressed in the hippocampal and anterior commissures as well as the corpus callosum. We also discuss the role of eutherian-specific *RTL1* in acquisition of the fine motor skill in eutherians by improving the function of corticospinal tract, presumably in association with the emergence of the eutherian-specific corpus callosum.

2 | RESULTS

2.1 | RTL1 expression in the human and mouse brain

We analyzed human *RTL1* expression by RT-PCR in several adult and fetal tissues as well as the placenta using commercially available human total RNA. *RTL1* was detected in the adult brain and cerebellum as well as the fetal brain at a very low level compared with the placenta and fetal liver: it was detected after 35 cycles of amplification (Figure 1). In the mice, a peak of *Rtl1* expression in the fetal brain was observed on embryonic day 12.5 (E12.5), but its level was also very low, as in the human brain, as 35 cycles of amplification were required to detect it. Moreover, its expression was much lower in E10.5 and E14.5 embryos and subsequently. The expression in the medulla oblongata and spinal cord increased in the later fetal stage, and the expression in the latter was observed also in the neonatal and adult stages after 32 cycles of amplification (Figure 1).

In the E12.5 brain (Figure 2), neural stem cells, the dorsal root ganglia (DRG), and Rathke's pouch, from which the anterior pituitary gland develops, were stained with the anti-RTL1 antibody. In the E14.5 brain, bundles of the nerve fibers were detected from the hindbrain region to the ventrolateral and dorsal spinal cord (Figure 2b,c), indicating that they contain neurons in the reticulospinal tract (RST) that connect the pons and medulla (hindbrain region) with spinal cord (Patestas & Gartner, 2016). In a series of sections of the neonatal brain (postnatal day 0 (P0)), we confirmed that the nerve bundles start from the somatomotor area of cerebral cortex layer V and run through the internal capsule and cerebral peduncles of the midbrain, pons, and medulla until they reach the spinal cord (Figure 2d–f), indicating that RTL1 is expressed in the pyramidal tract comprising the corticospinal (CST) and corticonuclear (CNT, also called corticobulbar) tracts in addition to the corticoreticular tract (CRT) that connects with the RST (Patestas & Gartner, 2016). The nerve bundles detected in the superior colliculus in the midbrain suggest that RTL1 is expressed in the corticotectal tract (CTT) from cerebral cortex layer V, whereas those in the thalamus suggest that it is also expressed in the corticothalamic tract (CThT) from cerebral cortex layer VI, suggesting an involvement in sensory processing (Briggs & Usrey, 2008).

In addition, the RTL1 protein was also detected in the commissural fibers connecting the corresponding regions in the

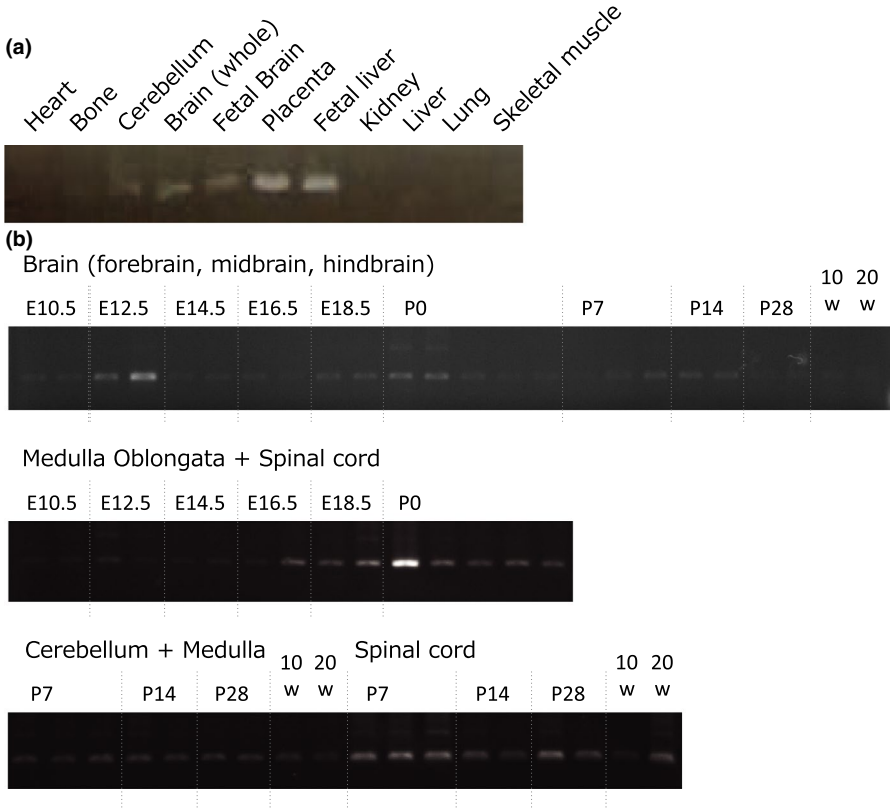

FIGURE 1 *Rtl1* mRNA expression in human and mouse brain. (a) PCR analysis of human *RTL1* in adult and fetal tissues and the following organs: the heart, bone, cerebellum, brain (whole), fetal brain, placenta, fetal liver, kidney, liver, lung, and skeletal muscle. (b) PCR analysis of mouse *Rtl1* in the brain, medulla oblongata, and spinal cords from E10.5 to 20 weeks of age

right and left hemispheres, such as the corpus callosum, hippocampal, and anterior commissures, as well as other structures in the limbic system, such as the *fimbria hippocami* (hippocampal fimbria), fornix, and medial amygdala nucleus (Figure 2d–f). We also analyzed RTL1 expression in the two types of disease model mice with paternal and maternal deletion of an *Rtl1* allele (Pat-*Rtl1*Δ and Mat-*Rtl1*Δ, respectively). In P0 neonates, a similar expression pattern in the brain was observed in the Pat-*Rtl1*Δ and Mat-*Rtl1*Δ mice (Figure 2g,h) compared with that of wild-type (WT) mice (Figure 2d–f). In the coronal section, RTL1 was detected in most of the corpus callosum, comprising the neurons from cortex layers V and VI, because the neurons from the cortical areas II and III make up only a minor population at this stage (P0) (Figure 2i) (Fame et al., 2011). Although the RTL1 protein was detected in Rathke's pouch in the E12.5 brain, it was not clearly detected in the pituitary gland in the E14.5 (and P0 brains) or P0 brain. The result from the RT-PCR experiment also demonstrated that *Rtl1* expression in the pituitary gland is not evident in the postnatal period (Appendix S1: Figure S2).

2.2 | Lack of RTL1 imprinted expression in the neonatal brain

Rtl1 is imprinted in the E14. 5 brain, like other tissues and organs, because its expression was completely lost in the Pat-*Rtl1*Δ brain, whereas being over-expressed in the Mat-*Rtl1*Δ brain (Appendix S1: Figure S3). However, as shown in Figure 2g, Pat-*Rtl1*Δretained brain expression despite of loss of expression in muscle tissues such as the tongue. The *Rtl1* mRNA level in the Pat-*Rtl1*Δ brain was approximately one half that of the wild type, indicating that *Rtl1* is also expressed from the maternally derived allele in the P0 brain (Figure 2j), whereas it was approximately two- to threefold higher in the Mat-*Rtl1*Δ brain than in WTm because of a lack of *antiRtl1* that degrades *Rtl1* mRNA through six microRNAs via an RNAi mechanism (Figure 2j) (Sekita et al., 2008; Kitazawa et al., 2017 and Kitazawa et al., 2020). Thus, it is likely that *Rtl1* imprinting is lost in the neonatal brain.

It should be noted that the two control mice, WTp and WTm (wild-type littermates with Pat-*Rtl1*Δ and Mat-*Rtl1*Δ, respectively: see Appendix S1: Figure S1), exhibited different levels of *Rtl1* expression: the latter being evidently lower than the former. In this and behavioral experiment, we excluded the neonatal lethal effects due to the B6 genetic background as well as the mother effects in generating the F1 (WTp and Pat-*Rtl1*Δ mice) and F2 (WTm and Mat- *Rtl1*Δ mice) generations to as great an extent as possible (Appendix S1: Figure S1). The former were generated by in vitro fertilization using eggs from wild-type females (Sv129) and F10 Pat-*Rtl1*Δ sperm (basically on a B6 background); then, the fertilized eggs were transplanted to pseudopregnant ICR females. Pups were born via Caesarian section and cared for by ICR surrogate mothers. The latter were generated by in vitro fertilization using eggs from F1 Pat-*Rtl1*Δ females and wild-type sperm (B6),

then transplanted into pseudopregnant ICR females, and the pups were cared for by ICR surrogate mothers after Caesarian section in like manner as in the former case. Therefore, it is likely that the different *Rtl1* expression was due to differences in the egg genotype used to generate the F1 and F2 generations (Sv129 for WTp and Pat-*Rtl1*Δ, 129/B6 F1 for WTm and Mat-*Rtl1*Δ), respectively.

2.3 | Reduction of locomotor activity, and incremental increase of anxiety-like and impaired fear conditioning behaviors in Pat-Rtl1Δ and Mat-Rtl1Δ mice

We subjected Pat-*Rtl1*Δ, Mat-*Rtl1*Δ mice, and their wild-type littermates (WTp and WTm) to a comprehensive

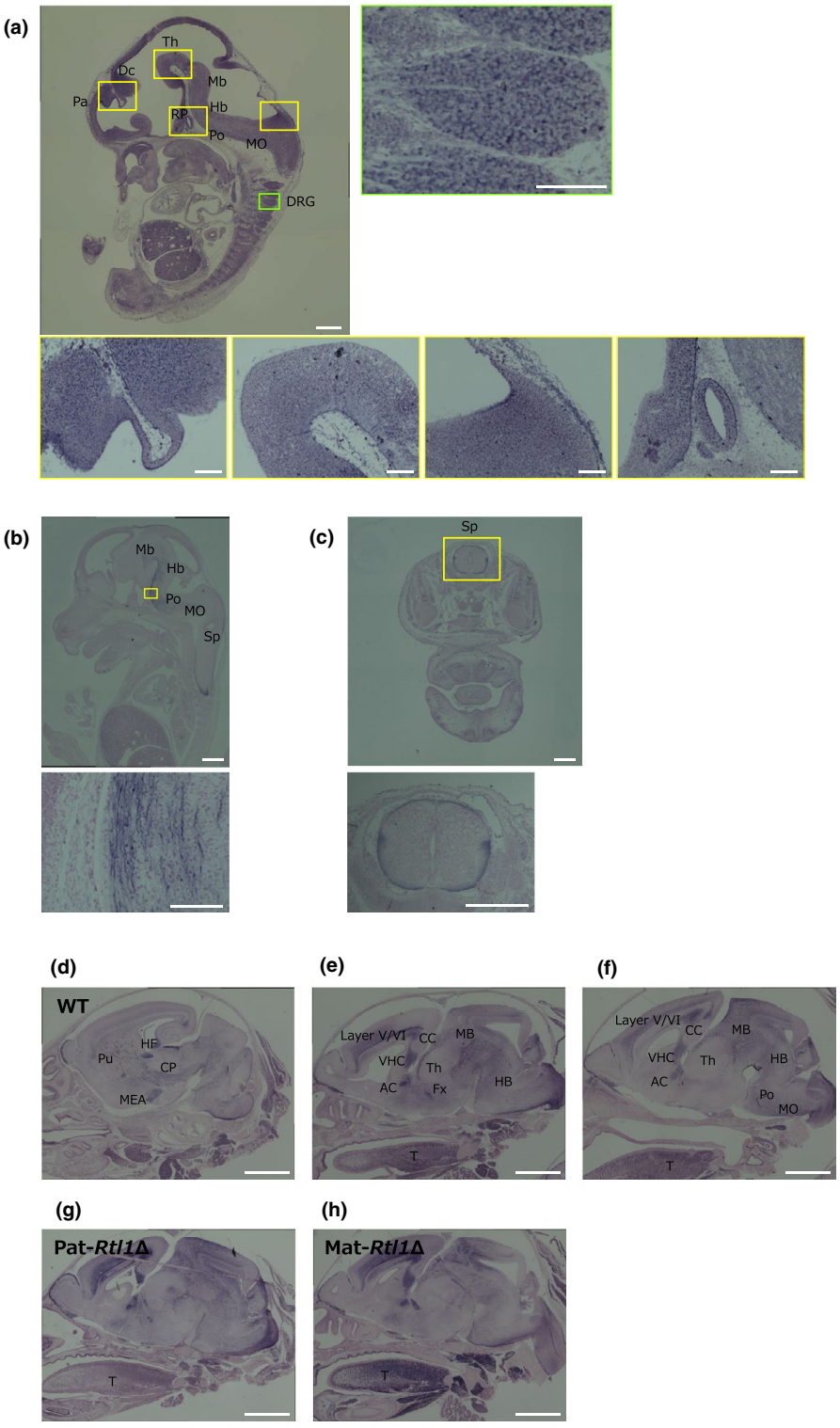

FIGURE 2 (Continued)

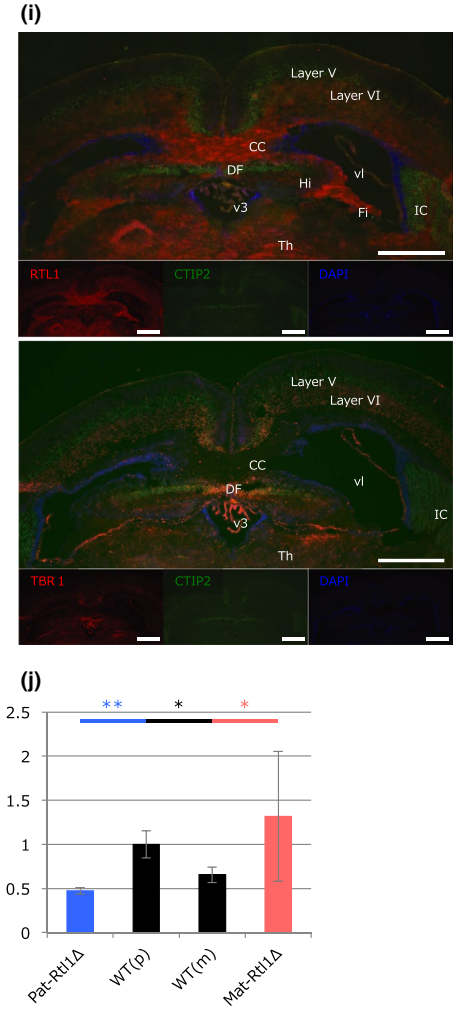

FIGURE 2 RTL1 expression in the nervous system during development. (a) A section of the entire E12.5 embryo (upper left) and magnified views of the dorsal root ganglion (upper right), telencephalon and prethalamus regions (lower left), the thalamus and pretectum regions (lower middle), and the hindbrain region (lower right). Scale bars: 500 μm (upper left), 100 μm (others). (b) A sagittal section of the entire E14.5 embryo (upper) and a magnified view of the prepontine hindbrain region (lower). Dc: diencephalon, DRG: dorsal root ganglion, Hb: hindbrain, Mb: midbrain, MO: medulla oblongata, Pa: pallium, Po: pons, RP: Rathke's pouch, Th: thalamus. Scale bars: 500 μm (top), 100 μm (bottom). (c) A coronal section of the E14.5 embryo (upper) and a magnified view of the spinal cord (lower). Scale bars: 500 μm. (d–f) A series of sagittal sections of the P0 neonatal brain (wild type). AC: anterior commissure, CC: corpus callosum, CP: cerebal peduncle, Hb: hindbrain, HF: hippocampal fimbria, MEA: Medial amygdala nucleus, Mb: midbrain, MO: medulla oblongata, Po: pons, Pu: putamen, T: tongue, VHC: ventral hippocampal commissure, layer V/VI: the fifth and sixth layers of cerebral cortex. (g, h) A sagittal section of the P0 neonatal brain of Pat-*Rtl1*Δ and Mat-*Rtl1*Δ, respectively, corresponding to section G (wild type). The RTL1 expression in tongue was much reduced in Pat-*Rtl1*Δ, as previously reported, whereas its brain expression remained the same and its expression was up-regulated in both the tongue and brain in Mat-*Rtl1*Δ. Scale bars: 1 mm. (i) A coronal section of the P0 neonatal brain. Upper: immunofluorescent staining of RTL1 (red), CTIP2 (green), and DAPI (blue). Lower: immunofluorescent staining of TBR1 (red), CTIP2 (green), and DAPI (blue). CC: corpus callosum, DF: dorsal fornix, Fi: fimbria, Hi: hippocampus, IC: internal capsule, layer V: the fifth layer of cerebral cortex, layer VI: the sixth layer of cerebral cortex, Th: thalamus, v3: the 3rd ventricle, vl; lateral ventricle. Scale bars: 500 μm. (j) *Rtl1* expression levels in P0 brain of Pat-*Rtl1*Δ (blue, $n = 2$), WTp (black, $n = 2$), WTm (black, $n = 2$), and Mat-*Rtl1*Δ (red, $n = 2$). Approximately one half of the level of *Rtl1* was expressed in the brain in the Pat-*Rtl1*Δ, indicating a loss of the imprinting regulation of *Rtl1* in the brain. * $p < .05$, ** $p < .01$. Two-tailed Student's *t*-test was used for the statistical analysis. Error bars indicate stdev

battery of behavioral tests to evaluate the behavioral effects of *Rtl1* under and over-expression, respectively. However, it should be noted that two wild-type mice exhibited different behavioral reactions in several tests (see the Discussion section).

Spontaneous locomotor activity was tested in the open field horizontal activity test. Both the Pat-*Rtl1*Δ and Mat-*Rtl1*Δ mice exhibited significant differences compared with the wild type in the parameters of total distance ($p = .0311$, $p = .0165$), average speed ($p = .0286$, $p = .0177$), and

distance per movement ($p = .07001$, $p = .0212$), whereas only the Mat-*Rtl1*Δ mice exhibited a significant difference on total movement duration ($p = .0526$, $p = .0477$) and the duration per movement ($p = .151$, $p = .0277$) (Figure 3a). However, we observed an apparent difference between WTp and WTm in the parameters of total movement duration ($p = .0313$) and total movement episode number ($p = .0412$) (see Appendix S1: Table S3). This suggests that Mat-*Rtl1*Δ mice also have an impaired total movement episode number compared with WT(p) mice and the difference in the effect observed on total movement duration seems more intense. In total, both Pat-*Rtl1*Δ and Mat-*Rtl1*Δ mice exhibited reduced spontaneous locomotor activity (both distance and speed), and the latter to a noteworthy extent. This trend was similarly observed in the other behavior tests described below.

In the elevated plus maze test, the Pat-*Rtl1*Δ mice displayed increased anxiety-like behavior. The total distance ($p = .0324$) and total entry number ($p = .0237$) were significantly decreased between Pat-*Rtl1*Δ and WT(p). The percentage of time spent in the open arm and the number of entries into the open arm were significantly decreased ($p = .0313$, $p = .0249$, respectively). Although the Mat-*Rtl1*Δ mice displayed no significant difference from WTm in these two parameters ($p = .425$, $p = .521$), there were significant differences between WTp and WTm in all of the 10 test parameters (see, Appendix S1: Table S4). These results suggest increased anxiety-like behavior in the Pat-*Rtl1*Δ, Mat-*Rtl1*Δ mice as well as the WTm mice (Figure 3b).

In the light/dark transition test, there was no significant difference between the Pat-*Rtl1*Δ and WTp in the distance in the dark or light chamber ($p = .0565$, $p = .0757$), but there was a significant difference between Mat-*Rtl1*Δ and WT(m) ($p = .00284$, $p = .0436$). There was no significant difference between the genotypes in terms of the time spent in the light chamber ($p = .234$, $p = .0774$) (see, Appendix S1: Table S5), but the number of transitions between the chambers was significantly decreased ($p = .0429$, $p = .0432$). These results suggest that anxiety-like behavior is mildly increased in both the Pat-*Rtl1*Δ and Mat-*Rtl1*Δ mice (Figure 3c).

In the fear conditioning test, there was also significant difference in total distance ($p = .0406$, $p = .00117$) but no significant difference between the genotypes and the WT in total freeze percentage ($p = .162$, $p = .0775$). In the contextual test (hippocampus-dependent memory retrieval) on the 2nd day, total freeze time was significantly increased between Mat-*Rtl1*Δ and WT(m) ($p = .0243$), but there was no significant difference between Pat-*Rtl1*Δ and WT(p) ($p = .276$). However, it should be noted that an apparent difference exists between WT(m) and WT(p) ($p = .0002$) that appears to be related to the difference between Mat-*Rtl1*Δ and WT(m) (see the Discussion section). In contrast, in the second cued test (amygdala-dependent memory retrieval) on the 3rd day, the total freeze percentage was significantly increased in both the Pat-*Rtl1*Δ and Mat-*Rtl1*Δ mice ($p = .0389$, $p = .0284$) (Figure 3d and Appendix S1: Table S6). This clearly indicates that both the Pat-*Rtl1*Δ and Mat-*Rtl1*Δ mice have impaired amygdala-dependent memory retrieval.

Hippocampal-dependent learning, induced acquisition of spatial memory, and long-term spatial memory were tested in the Morris water maze test. There were significant differences in total distance and moving speed between Mat-*Rtl1*Δ and WTm ($p = .0168$, $p = .00376$). Importantly, Mat-*Rtl1*Δ mice did not exhibit any improvement during the period of the first and fourth day of the experiments in terms of the time to reach the platform, indicating that the Mat-*Rtl1*Δ mice had severely impaired spatial memory in addition to reduced locomotor activity, whereas Pat-*Rtl1*Δ displayed an excellent performance on this test, indicating that Pat-*Rtl1*Δ have better memory than WTp, or, alternatively, they may have increased escape behavior (Figure 3e and Appendix S1: Table S7).

3 | DISCUSSION

We found that *Rtl1* expression in the fetal brain was very low by RT-PCR analysis, but the immunohistological analyses using an anti-RTL1 protein clearly illustrated the precise RTL1 expression profiles in the CNS from E12.5 to P0, demonstrating that RTL1 is actually expressed in the pyramidal tract comprising CST and CNT as well as CRT and RST that regulate the motor and sensory neurons in the limbs and trunk from cortex layer V (Patestas & Gartner, 2016) as well as in the CTT, which together with the CRT works in parallel with the CST to influence motoneurons in the spinal cord both directly and indirectly *via* the brainstem descending pathways (Fregosi et al., 2019). RTL1 is also expressed in the CThT from layer VI, an integral part of thalamo-cortico-thalamic circuit which intimately interconnects the thalamus and cortex for sensory processing (Briggs & Usrey, 2008). RTL1 is also expressed in the interhemispheric commissural structures, such as the corpus callosum, hippocampal, and anterior commissures that communicate with the corresponding right and left hemispheric sites (Mihrshahi, 2006; Suárez et al., 2014), and the hippocampal fimbria and fornix, the major output route of hippocampal-related memory formation (Warburton et al., 2000; Aggleton & Nelson, 2015), and the medial amygdala nucleus, a structure involved in emotion-related behavior (Pardo-Bellver et al., 2012). Therefore, we think it is highly likely that the resulting impairment of these brain and spinal functions leads to the neurological defects that are observed in KOS14 and TS14 patients, although it remains to be determined whether humans have the same RTL1 expression profiles in the nervous system. In general, it is very challenging to reproduce human neurological phenotypes (i.e., symptoms) solely with data from behavioral

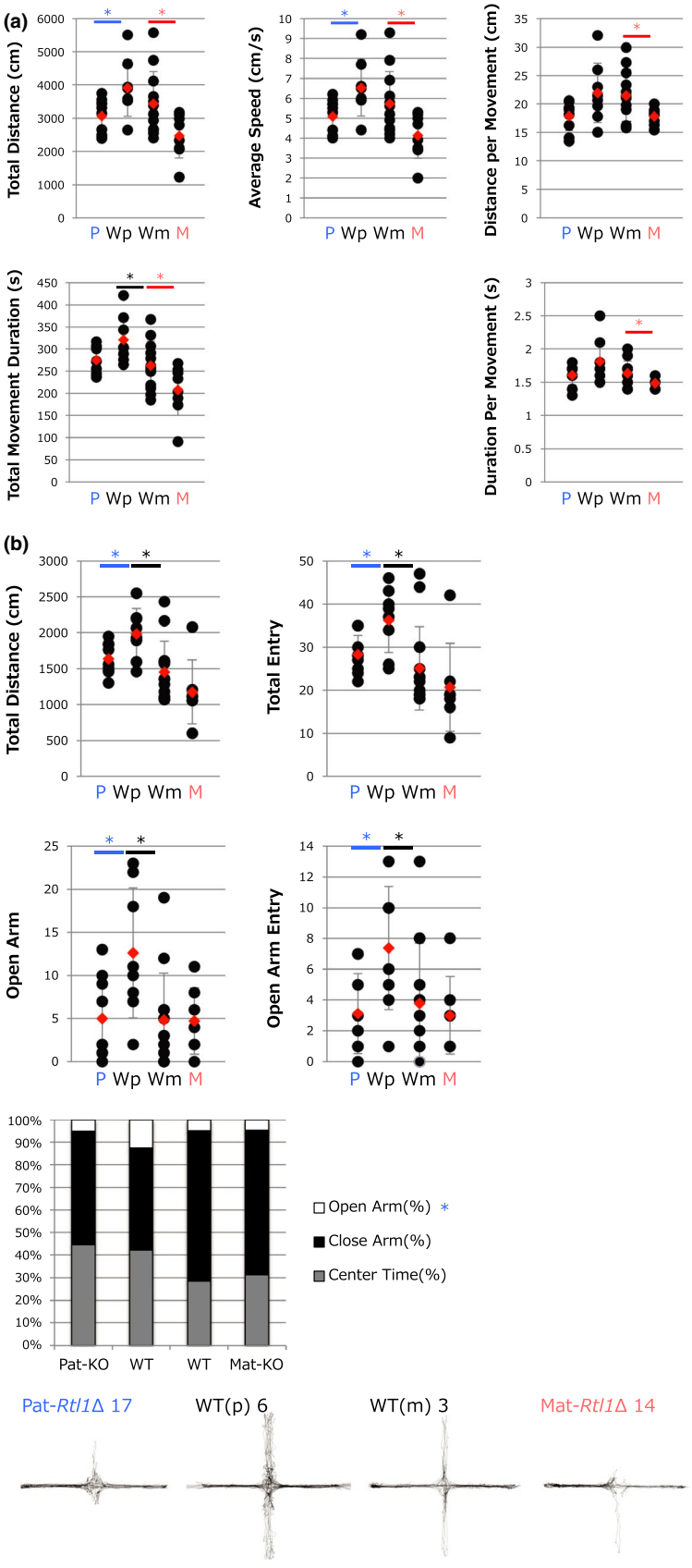

FIGURE 3 (Continued)

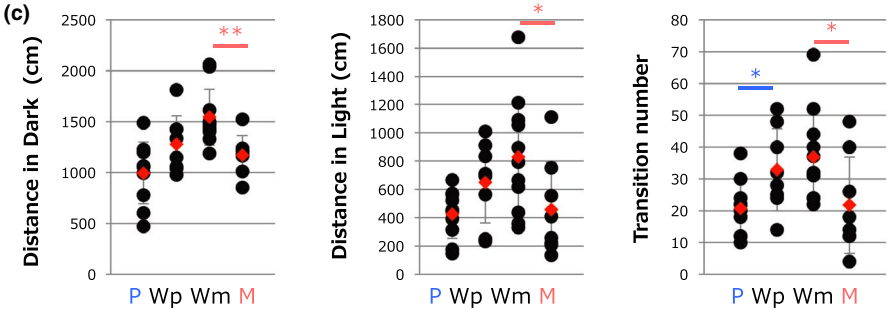
(c)
Distance in Dark (cm)
Distance in Light (cm)
Transition number
P Wp Wm M

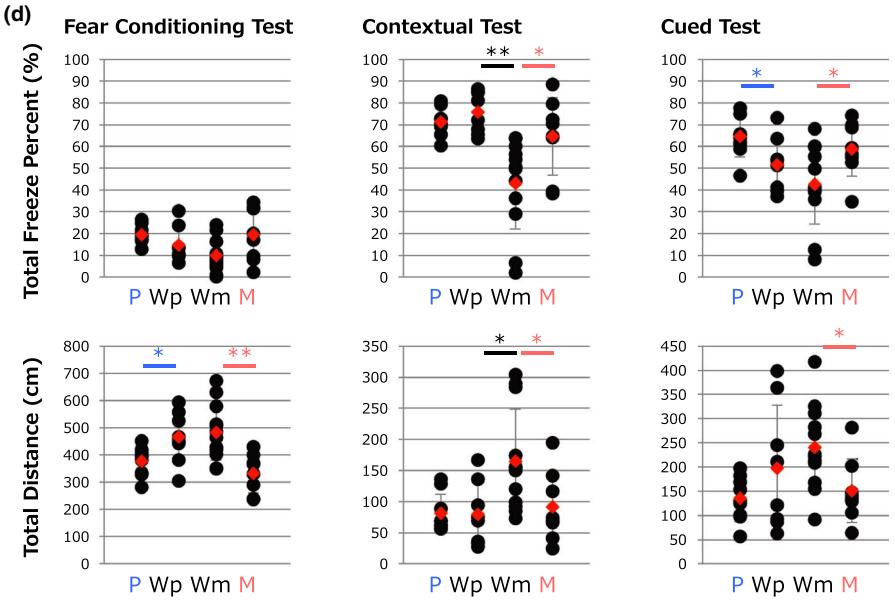
(d)
Fear Conditioning Test
Contextual Test
Cued Test
Total Freeze Percent (%)
Total Distance (cm)
P Wp Wm M

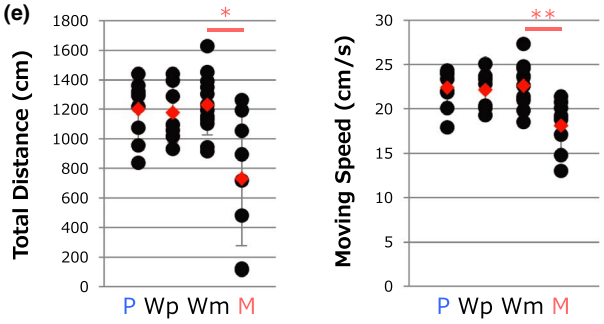
(e)
Total Distance (cm)
Moving Speed (cm/s)
P Wp Wm M

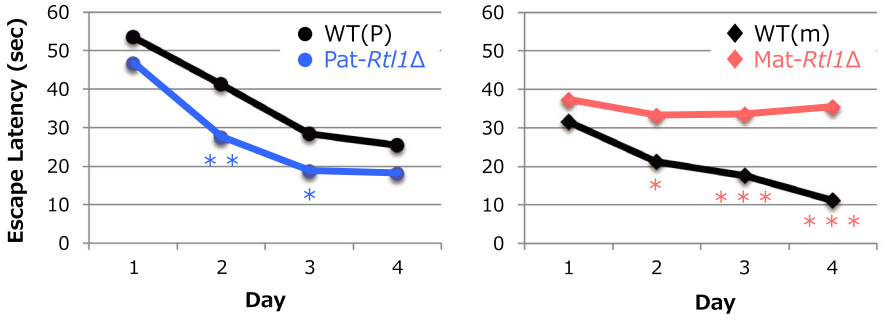
Escape Latency (sec)
WT(P)
Pat-Rtl1Δ
WT(m)
Mat-Rtl1Δ
Day

FIGURE 3 Behavioral abnormalities in Pat-*Rtl1*Δ and Mat-*Rtl1*Δ mice. (a) Open field test at 9 w. The results of total distance, average speed, distance per movement, total movement duration, and duration per movement are shown. The data points are depicted as black circles, and their means ± S. E. M. (n = 10, 8, 11, and 8, respectively) are represented as red diamonds. The asterisk indicates significant differences between the WTp and Pat-*Rtl1*Δ (blue), WTm and Mat-*Rtl1*Δ (red), and WTp and WTm mice (black) (*: $p < .05$, **: $p < .01$). (b) Elevated plus maze test. The results of total distance, total entry, open arm time, and open arm entry are shown. The data points are depicted as black circles, and their means ± S. E. M. (n = 10, 8, 11 and 8, respectively) are represented as red diamonds. The asterisk indicates significant differences between the WTp and Pat-*Rtl1*Δ (blue), WTm and Mat-*Rtl1*Δ (red), and WTp and WTm mice (black) (*: $p < .05$, **: $p < .01$). The percentages of their center, open arm and close arm are independently shown as a bar graph. A trajectory of each one of the examples in this experiment is also represented. (c) Light/Dark transition test. The results of distance in the dark, distance in the light, and total transition number are shown. The data points are represented as black circle and their means ± S. E. M. (n = 10, 7, 10, and 8, respectively) as red diamonds. The asterisk indicates significant differences between the WTp and Pat-*Rtl1*Δ (blue), WTm and Mat-*Rtl1*Δ (red), and WTp and WTm mice (black) (*: $p < .05$, **: $p < .01$). (d) Fear conditioning test. The results of total freeze percentage and total distance are shown for the first day (fear conditioning test), second day (contextual test), and third day (cued test), respectively. The data points are represented as black circles and their means ± S. E. M. (n = 10, 8, 11, and 8, respectively) as red diamonds. The asterisk indicates significant differences between the WTp and Pat-*Rtl1*Δ (blue), WTm and Mat-*Rtl1*Δ (red), and WTp and WTm mice (black) (*: $p < .05$, **: $p < .01$). (e) Morris water maze test. The results of total distance and moving speed are shown. The data points are represented as black circles and their means ± S. E. M. (n = 10, 8, 11, and 8 each, respectively) as red diamonds. The asterisk indicates significant differences between the WTp and Pat-*Rtl1*Δ (blue), WTm and Mat-*Rtl1*Δ (red), and WTp and WTm mice (black) (*: $p < .05$, **: $p < .01$). The escape latency (sec) of WTp (black) and Pat-*Rtl1*Δ (blue) (left) as well as WTm (black) and Mat-*Rtl1*Δ (blue) (right) are also presented. Each data point represents the mean ± S. E. M. (n = 10 and 8, 11, and 8, respectively). The asterisk indicates significant differences between the WTp and Pat-*Rtl1*Δ (blue), and WTm and Mat-*Rtl1*Δ (red) (*: $p < .05$, **: $p < .01$, ***: $p < .001$)

analyses of KO mice, even when they display the same genetic defects. In an effort to overcome the evident limitation of the behavior tests using the Mat- and Pat *Rtl1*ΔKO mice, it is reasonable to consider the symptoms of KOS14 and TS14 in the context of the results from these KO mice with the help of the comprehensive RTL1 expression profiles in the CNS described above.

Most KOS14 patients exhibit developmental delay/intellectual disability and feeding difficulties, whereas approximately 2/3 of TS14 patients exhibit hypotonia and feeding difficulties, and some exhibit auditory impairment (Kotzot, 2004; Kagami et al., 2005, 2008, 2015, and Kagami et al. 2016; Ioannides et al., 2014; Ogata & Kagami, 2016). As expected, it has proven to be very difficult to straightforwardly account for most of these symptoms only from the behavioral abnormalities observed in the KO mouse models with over- and under-expression of *Rtl1*. However, the feeding difficulties and delayed speech might be explained by the impairment of certain cranial nerves, such as the trigeminal (the fifth of cranial nerve, V), glossopharyngeal (IX), vagus (X), and hypoglossal (XII) nerves, and the auditory impairment by the vestibulocochlear (VIII) nerves because the CNT directly innervate these cranial nerves (Patestas & Gartner, 2016). It may be possible that the impairment of the oral cavity as well as tongue muscles linked to these symptoms, as we previously reported that RTL1 is expressed in fetal/neonatal skeletal muscles. However, it is also possible that impairment of cranial nerves regulating the oral and tongue muscles plays a role in these symptoms. It is yet again possible that some combination of both is the case.

Concerning the motor delay, the two mouse models exhibited a severe reduction in locomotive activity in most of the behavioral tests. Therefore, this is highly likely to be associated with the impairment of CST, CRT, and RST because they are responsible for the voluntary muscle movement of the trunk and limbs (Lemon, 2008; Patestas & Gartner, 2016), such as specific skilled muscle movement (i.e. CST) (Iwaniuk & Whishaw, 2000) and diverse specific motor function (i.e., CRT and RST) (Perreault & Giorgi, 2019) including escape, micturition, reaching and grasping, sleep, respiration, vomiting, and locomotion. Impairment of the corpus callosum is also likely to be involved in the motor delay because it connects the right and left hemispheres and is critically involved in information exchange, especially in cortex layer V.

In our most recent published report, we discussed the fact that skeletal muscles defects, especially in the muscles used in respiration, such as the diaphragm, intercoastal, and abdominal muscles, are the major cause of respiratory problem leading to neonatal lethality in KOS14 patients. However, the findings in this work, that *Rtl1* expression was clearly observed in the CST, CRT, and RST, suggesting that impairment in spinal nerves, such as the phrenic nerve (C3 ~ 5) innervating the diaphragm and thoracic nerve (Th1 ~ 11) innervating the internal and external intercoastal muscles as well as abdominal muscles, are involved in the respiratory defects. Similarly, we previously proposed that the hypotonia observed in neonatal TS14 patients is caused by defects in trunk muscle development, but it seems likely that this hypotonia is also caused by neonate-specific transient neuromuscular defects, because they eventually outgrow the condition.

In terms of developmental delay/intellectual disability, it is possible that RTL1 expression in the hippocampal fimbria and fornix as well as medial amygdala nucleus is related to this symptom. The fimbria and fornix are the main output routes of hippocampus memory (Warburton et al., 2000;

Aggleton & Nelson, 2015), and the medial amygdala nucleus is a key structure in the emotional response by relaying olfactory information to the hypothalamic nuclei involved in reproduction and defense (Pardo-Bellver et al., 2012; Keshavarzi et al., 2014). Memory and social behavior are essential parts of behavioral development as well as intellectual disabilities (Darling-Hammond et al., 2020). This characterization is consistent with the finding that the two mouse models exhibited increased anxiety, as well as impaired amygdala- and possibly hippocampus-dependent fear responses. It is also supported by the evidence that most knockout mice related to the intellectual disability genes in humans exhibited impaired score in the fear conditioning test (Zhang et al., 2015; Aincy et al., 2018). In the behavioral tests, WTp and WTm mice exhibited different phenotypes, especially in that WTm mice exhibited severe responses in the elevated plus maze and fear conditioning tests compared with the WTp mice. As mentioned above, there is an egg genotype difference between WTp (Sv129) and WTm (Sv129/B6 F1). However, it is unlikely that such a difference would affect only the results of the elevated plus maze and fear conditioning tests. As the Mat-*Rtl1*Δ pups displayed much more severe responses in the fear conditioning test than the WTm mice, we assume that this was the result of the Mat-*Rtl1*Δ pups having been raised together with the WTm mice before weaning at 4 weeks of age. They may suffer from exposure to the abnormal behavior of the Mat-*Rtl1*Δ pups in a specific manner, especially in terms of fear conditioning. *Rtl1* expression in the WTm mice was lower than the WTp mice, it is possible that this may be related to their sensitivity to the abnormal behavior of their littermates.

Concerning the postnatal growth retardation observed in the TS14 patients, the Pat-*Rtl1*Δ pups maintained a lower weight than the control WTp pups (Sekita et al., 2008; Kitazawa et al., 2017). Similarly, KO mice with delta like noncanonical Notch ligand 1(*Dlk1*) in the same imprinted region exhibited postnatal growth retardation (Moon et al., 2002; Cheung et al., 2013). Therefore, it is highly likely that both *RTL1* and *DLK1* are related to the postnatal growth retardation of TS14, although the crown-rump length of Pat-*Rtl1*Δ pups recovered to the same level in the period from weaning period to 8 weeks (Kitazawa et al., 2017) and the effect of *Dlk1* KO was slight concerning the body length in the period from weaning to 14 weeks (Cheung et al., 2013). TS14 patients exhibit a postnatal reduction in both body weight and length (Ioannides et al., 2014; Kagami et al., 2017), suggesting that the effects of *RTL1/Rtl1* and *DLK1/Dlk1* are different in humans and mice or that other maternally expressed imprinted genes, such as *MEG3*, *MEG8,* and *MEG9,* may contribute to the postnatal growth retardation as well as other symptoms in TS14 and KOS14. Alternatively, concomitant loss of both *RTL1* and *DLK1* genes may be necessary to explain the reduced postnatal body length. *Rtl1* expression in the pituitary gland was not as evident in mice (Figure 2j), whereas *Dlk1* exhibits apparent pituitary gland expression in the pre- and postnatal periods (Yevtodiyenko & Schmidt, 2006; Cheung et al., 2013; Falix et al., 2013). *Dlk1*KO mice also exhibit a mild reduction in pituitary growth hormone (GH) content in the postnatal period, although it is believed that such mild GH reduction is inadequate to explain the postnatal growth retardation in *Dlk1* KO mice (Cheung et al., 2013). Thus, the real cause of postnatal growth retardation in both *Rtl1* and *Dlk1* KO mice remains to be elucidated.

It is of interest that eutherian-specific RTL1 (Charlier et al., 2001; Edwards et al., 2008; Kaneko-Ishino & Ishino, 2012, 2015) is expressed in both the corticospinal tract and corpus callosum, that is, mammalian- and eutherian-specific brain structures, respectively (Aboitiz & Montiel, 2003; Mihrshahi, 2006; Suárez et al., 2014). The corticospinal tract is responsible for fine muscle movement, and it is reported that the eutherian corticospinal tract system is functionally superior to that in marsupials by comparing the paw skills of rats and opossums (Frost et al., 2000; Ivanco et al., 1996), implying that RTL1 may play a role in the evolution of this system as a eutherian-specific gene. The corpus callosum connects the left and right brain hemispheres, so it is highly probable that the emergence of corpus callosum also contributed to the improvement of skilled motor function along with other behaviors (Mihrshahi, 2006; Suárez et al., 2014). It is comprised of nerve fibers derived mainly from the cerebral cortex layers II and III in the upper layer as well as in the lower portion of cerebral cortex layers V and VI in adults (Fame et al., 2011), where RTL1 is specifically expressed. It is of great interest that RTL1 is also expressed in the hippocampal commissure, implying that RTL1 might have been involved in the evolutionary emergence of this structure, because it has been suggested that the evolution of the corpus callosum involved a rerouting of dorsal cortical axons. This rerouting involves axons crossing through the anterior commissure that employ the same embryonic substrate as the hippocampal commissure and the fact that the nerve fibers in the hippocampal commissure connecting the left and right fornix help the nerve fibers in the corpus callosum pass though the midline of the brain on embryonic development day 15.5 (E15.5) (Mihrshahi, 2006; Suárez et al., 2014).

Rtl1 imprinting is lost in the P0 brain, so one half of the *RTL1* expression, from the maternal allele, was observed in the P0 Pat-*Rtl1*Δ brain. Importantly, *Rtl1* is apparently imprinted in the E14. 5 brain, like other tissues and organs, because its expression was completely lost in the Pat-*Rtl1*Δ brain whereas being over-expressed in the Mat-*Rtl1*Δ brain (Appendix S1: Figure S2). A similar result was previously reported in which *Dlk1* imprinting is lost in postnatal stem cells and the niche astrocytes regulating neurogenesis

(Ferrón et al., 2011), suggesting that the postnatal loss of genomic imprinting in the brain might be a characteristic of the *DLK-DIO3* imprinted region. Although the molecular function of RTL1 in the brain as well as the details in the neuronal impairments that result from its irregular expression remain to be elucidated, these findings suggest that KOS14 and TS14 should be regarded as neuromuscular as well as neuropsychiatric diseases caused by over- and under-expression of *RTL1*, although the hypotonia in TS14 is transient and neonate-specific. It also implies that eutherian-specific *RTL1* might be a key gene in the functional evolution of eutherian nerve system. Thus, *RTL1* is another good example of acquired genes from LTR-retrotransposons and/or retroviruses functioning in the eutherian brain, such as *Arc* (Campillos et al., 2006; Ashley et al., 2018; Pastuzyn et al., 2018), *Sirh11/Zcchc16* (also termed *Rtl4*) (Irie et al., 2015, 2016), *Rtl6* (also termed *Sirh3/Ldoc1l*), and *Rtl5* (also termed *Sirh8/Rgag1*)(submitted) in addition to the placenta (Sekita et al., 2008) like *SYNCYTINEs* (Mi et al., 2000; Lavialle et al., 2013), *Fematrin-1*(Nakaya et al., 2013), *PEG10* (Ono et al., 2001, 2006), and *Sirh7/Ldoc1* (also termed *Rtl7*) (Naruse et al., 2014; Kaneko-Ishino & Ishino, 2012, 2015).

4 | EXPERIMENTAL PROCEDURES

4.1 | Mice

All animals and experimental procedures were approved by the Animal Ethics Committees of Tokyo Medical and Dental University. The *Rtl1* KO mice were generated by using ES cells (CCE) of 129/SvEv mouse origin, as previously described (Sekita et al., 2008). The *Rtl1* KO lines were maintained by continuous crossing with male and female C57BL/6J mice (WT), and mice in the F1 (*Rtl1* KO: Pat-*Rtl1*Δ) and F2 (*antiRtl1as* KO: Mat-*Rtl1*Δ) generations were used for behavioral analyses, whereas the F8 (Pat-*Rtl1*Δ) and F9 (Mat-*Rtl1*Δ) generations were used for immunohistochemical analyses.

4.2 | Analysis of the expression of *RTL1/Rtl1*

The human total RNA set was purchased from TOYOBO (Japan, Master Panel II, Clontech catalog no. 636,643). The cDNA was synthesized from 1μg of total RNA using ReverTra Ace® qPCR RT Master Mix (TOYOBO) according to the manufacturer's protocol. For the RT-PCR analysis of *RTL1*, 10 ng of cDNA in a 25 μl reaction mixture containing 1x ExTaq buffer (TAKARA), 200 μM of each dNTP, primers and 0.5 units of ExTaq HS (TAKARA) were subjected to 35 cycles at 98℃ for 10 s, 60℃ for 30 s, and 72℃ for 30 s using a C1000 Touch thermal cycler (Biorad). The following primer sequences were used: a *RTL1 forward primer*, 5'- AACCCACTTGTGAAGGGCAA-3'; a reverse primer, 5'- CCTCATGGATGTCACTCCCG-3'. The genomic DNA and total RNA samples were prepared from fetuses, neonates, and 1- and 4-week-old mice using TRIzol Regent (Life Technologies). The cDNA was synthesized from 5 μg of total RNA using SuperScript III Reverse Transcriptase (Invitrogen) with the following oligo-dT + Adaptor primer: 5'-CTGATC TAGAGGTACCGGATCCGACTCGAGTCGACATCGTT TTTTTTTTTTTTTTT-3'. For the RT-PCR analysis of *Rtl1*, 10 ng of cDNA in a 25 μl reaction mixture containing 1x KOD FX buffer (KFX-101, TOYOBO), 200 μM of each dNTP, primers, and 0.5 units of KOD FX was subjected to 30 cycles at 98℃ for 15 s, 69℃ for 30 s, and 74℃ for 30 s using a C1000 Touch thermal cycler (Biorad). The following primer sequences were used: *Rtl1*, 5'-TCCAAGGAGCATTCGAC GTACCAGTGTGACTTACC-3'; an adaptor primer for both genes, 5'-AGAGGTACCGGATCCGACTCGAGTCGACA TCG-3'; and *Gapdh*, 5'-CACTCTTCCACCTTCGATGC-3' and 5'-CTCTTGCTCAGTGTCCTTGC-3'.

4.3 | Quantitative PCR assay

The quantitative real-time PCR was performed by using 5 ng of cDNA in a THUNDERBIRD SYBR qPCR Mix (QPS-201, TOYOBO). The cycle conditions were 95℃ for 1 min, followed by 40 cycles of 95℃ for 10 s, 60℃ for 20 s and 72℃ for 10 s using the LightCycler 480 apparatus (Roche). The gene expression levels were normalized to *Gapdh*. The following primer sequences were used for this study: *Rtl1,* 5'-GAGTACTGTGCCAAGGAGCC-3' and the Adaptor primer described above.

4.4 | Immunostaining (paraffin sections)

Mouse fetuses and neonates were fixed using SUPER FIX (KURABO), soaked in 5% formic acid in 70% ethanol at 4℃ overnight for two nights, dehydrated in 70% and 90% ethanol for 2 hr each, 100% ethanol for 2 hr three times, and xylen for 2 hr four times, and finally embedded in paraffin wax. The paraffin blocks were sectioned at a 5-μm thickness with a microtome and mounted on Superfrost Micro Slides (Matsunami Glass). The sections were deparaffinized 3 times in xylene for 20 min, 3 times in 100% ethanol for 5 min, and in 90% and 70% ethanol for 5 min each. For antigen retrieval, the sections were boiled in 0.01 M Citrate Buffer pH 6.0 at 98℃ for 40 min and then immersed (dehydrated) in cold methanol at −30℃ overnight. After being air dried, the sections were blocked with 10% goat serum, 5% bovine serum albumin (BSA: Sigma

Aldrich), and 0.1% Triton-X 100 (WAKO) in PBS at room temperature for 1 hr.

For the immunohistochemical analysis, an anti-Rtl1 antibody (1:200) was used as the primary antibody and was prepared in 5% BSA and 0.1% Triton-X 100 in PBS at 4℃ overnight (more than 20 hr). This primary reaction was developed with a biotinylated goat anti-rabbit IgG secondary antibody (1:200; Vector Laboratories) for 2.5 hr and then incubated with an alkaline phosphatase (AP) complex (1:200; Vector Laboratories) for 1 hr. The histochemical detection of the alkaline phosphatase activity was performed with BCIP/NBT (Vector Laboratories) in 100 mM Tris-HCl at a pH of 9.8 and mounted with VectaMount AQ Mounting Medium (Vector Laboratories). The images were captured using **a** BIOREVO microscope (KEYENCE).

4.5 | Immunostaining (Cryosections)

Mouse neonate brains were corrected and fixed in 4% paraformaldehyde (PFA: Nacalai tesque), 10% and 25% sucrose at 4℃ overnight each and finally embedded in OCT compound (Sakura Finetek). The OCT blocks were sectioned at a 12-μm thickness with a cryostat (MICROTOME) and mounted on Superfrost Micro Slides (Matsunami Glass). The cryosections were fixed in 4% PFA for 10 min at room temperature and washed three times with PBS for 5 min. For antigen retrieval, the sections were boiled in 0.01 M Citrate Buffer pH 6.0 at 80℃ for 10 min and then immersed (dehydrated) in cold methanol at −30℃ 7 min. After being air dried, the sections were blocked with 10% goat serum, 5% bovine serum albumin (BSA: Sigma Aldrich), and 0.1% Triton-X 100 (WAKO) in PBS at room temperature for 1 hr.

For the immunofluorescence staining, anti-Rtl1 antibody (1:200), anti-Ctip2 antibody (1:500, abcam), and anti-Tbr1 antibody (1:500, abcam) were used as the primary antibody and was prepared in 5% BSA and 0.1% Triton-X 100 in PBS at 4℃ overnight (approximately 16 hr). Alexa Fluor 488-conjugated anti-mouse IgG (1:1,000, Thermo Fisher Scientific) and 555-conjugated anti-rabbit IgG (1:1,000, Thermo Fisher Scientific) were used as the secondary antibodies and stained with DAPI (1:1,000, WAKO) for 1 hr. The slides were mounted with VectaShield (Vector Laboratories). The images were captured using a BIOREVO microscope (KEYENCE).

4.6 | Open field test

Locomotor activity was measured using an open field test. Each mouse was placed in the corner of the open field apparatus (40 x 40 x 30 cm; Accuscan Instruments, O'hara & Co., LTD.). The chamber of the test was illuminated at 100 lux. Total distance travelled (in cm), vertical activity, and time spent in the center area were recorded. Data were collected for 10 min using a video camera attached to a computer and were calculated by the Image OF program.

4.7 | Elevated plus maze test

The elevated plus maze consisted of two open arms (25 x 5 cm) and two closed arms of the same size with 15 cm high transparent walls (O'hara & Co., LTD.). The arms and central square were made of gray plastic plates and were elevated 50 cm above the floor. The behavior testing room (170 x 210 x 200 cm) was soundproof, and the illumination level was maintained at 100 lux. Each mouse was placed in the central square of the maze with its head toward a closed arm. Data were recorded for 10 min using a video camera attached to a computer and were calculated by the Image EP program. The number of entries into each arm and the time spent in the open arms were recorded, and these measurements served as an index of anxiety-like behavior.

4.8 | Light/dark transition test

The apparatus used for the light/dark transition test comprised a cage (21 x 42 x 25 cm) divided into two sections of equal size by a partition with a door (O'hara & Co., LTD.). One chamber was brightly illuminated (400 lux), whereas the other chamber was dark. Each mouse was placed into the dark side and allowed to move freely between the two chambers with the door open for 10 min. The total number of transitions between the chambers, the time spent in each, the latency to first enter the light chamber, and the distance travelled in each chamber were recorded using a video camera attached to a computer and calculated by the Image LD program.

4.9 | Contextual and cued fear conditioning test

On the 1st day, each mouse was placed into a test chamber (26 x 34 x 29 cm) with a stainless-steel grid floor inside a sound-attenuated chamber and allowed to explore freely for 2 min. A 60 db white noise, which served as the conditioning stimulus (CS), was presented for 30 s, followed by a mild foot shock (2 s, 0.5 mA), which served as the unconditioned stimulus (US). Two more CS-US pairings were presented with a 2 min interstimulus interval. On the 2nd day, a context test was conducted in the same chamber as the conditioning test and data were recorded for 2 min. On the 3rd day, a cued test was conducted in the white opaque plastic chamber and the same 60 db white noise as used on the 1st day was presented for 30 s and data were recorded for 2 min using a

video camera attached to a computer. In each test, the movement freezing percentage and distance travelled were calculated automatically by the Image FZ program.

4.10 | Morris water maze test

The apparatus used for the Morris water maze test was a circular pool with a diameter of 100 cm and depth of 50 cm. Four high contrast spatial cues were placed about the room (above the pool). A 10-cm diameter clear plexiglass platform was placed in the pool and the pool filled with water until the platform was 1 cm above the water surface. The water was allowed to equilibrate to room temperature (22℃) and the white paint melted so as to make the water in the pool cloudy. Each mouse was put into a location which the computer had specified. During the 1st to 4th days, the maximum trial time was set at 60 s and if mouse found the platform before this time, the program software stopped the trial. On the 5th day, 1 trial was created with no platform zone and the mouse was allowed to swim for 60 s. Data were recorded using a video camera attached to a computer, and the data were calculated automatically by the Image MWM program.

ACKNOWLEDGMENTS

We thank Drs. Y. Sekita (Kitasato University, School of Science), D. Endo (Nagasaki University, Graduate School of Biochemical Science), H. Shiura (the University of Yamanashi) and J. Lee (TMDU) for their helpful advice. Pacific Edit reviewed the manuscript prior to submission.

CONFLICT OF INTEREST

The authors have declared that no competing interests exist.

AUTHOR CONTRIBUTIONS

T.K.-I. and F.I. conceived and designed the experiments; M.K. and A.S. performed the experiments; M.K. analyzed KO mice and performed the immunofluorescence analyses; M.K., A.S., T.K.-I., and F.I. analyzed the data and drafted the manuscript.

ORCID

Tomoko Kaneko-Ishino https://orcid.org/0000-0002-2566-9961
Fumitoshi Ishino https://orcid.org/0000-0001-8458-6069

REFERENCES

Aboitiz, F., & Montiel, J. (2003). One hundred million years of interhemispheric communication: The history of the corpus callosum. *Brazilian Journal of Medical and Biological Research*, *36*, 409–420.

Aggleton, J. P., & Nelson, A. J. D. (2015). Why do lesions in the rodent anterior thalamic nuclei cause such severe spatial deficits? *Neurosci Biobehavior Reviews*, *54*, 131–144.

Aincy, M., Mezianec, H., Herault, Y., & Humeau, Y. (2018). Synaptic dysfunction in amygdala in intellectual disorder models. *Prog Neuropsychopharmacol and Biol Psychiat*, *84*, 392–397.

Ashley, J., Cordy, B., Lucia, D., Fradkin, L. G., Budnik, V., & Thomson, T. (2018). Retrovirus-like Gag Protein Arc1 Binds RNA and Traffics across Synaptic Boutons. *Cell*, *172*, 262–274.

Briggs, F., & Usrey, W. M. (2008). Emerging views of corticothalamic function. *Current Opinion in Neurobiology*, *18*, 403–407.

Campillos, M., Doerks, T., Shah, P. K., & Bork, P. (2006). Computational characterization of multiple Gag-like human proteins. *Trends in Genetics*, *22*, 585–589.

Charlier, C., Segers, K., Wagenaar, D., Karim, L., Berghmans, S., Jaillon, O., & Georges, M. (2001). Human–Ovine Comparative Sequencing of a 250-kb Imprinted Domain Encompassing the Callipyge (clpg) Locus and Identification of Six Imprinted Transcripts: *DLK1*, *DAT*, *GTL2*, *PEG11*, *antiPEG11*, and *MEG8*. *Genome Research*, *11*, 850–862.

Cheung, L. Y. M., Rizzoti, K., Lovell-Badge, R., & Le Tissier, P. R. (2013). Pituitary phenotypes of mice lacking the notch signalling ligand delta-like 1 homologue. *Journal of Neuroendocrinology*, *25*, 391–401.

Darling-Hammond, L., Flook, L., Cook-Harvey, C., Barron, B., & Osher, D. (2020). Implications for educational practice of the science of learning and development. *Applied Developmental Science*, *24*(2), 97–140.

Edwards, C. A., Mungall, A. J., Matthews, L., Ryder, E., Gray, D. J., Pask, A. J., & Ferguson-Smith, A. C.(2008). The evolution of the DLK1-DIO3 imprinted domain in mammals. *PLoS Biology*, *6*, e135.

Falix, F. A., Tjon-A-Loi, M. R. S., Gaemers, I. C., Aronson, D. C., & Lamers, W. H. (2013). DLK1 Protein Expression during Mouse Development Provides New Insights into Its Function. *ISRN Developmental Biology*, *2013*, 628962.

Fame, R. M., MacDonald, J. L., & Macklis, J. D. (2011). Development, Specification, and Diversity of Callosal Projection Neurons. *Trends in Neurosciences*, *34*, 41–50.

Ferrón, S. R., Charalambous, M., Radford, E., McEwen, K., Wildner, H., Hind, H., & Ferguson-Smith, A. C. (2011). Postnatal loss of Dlk1 imprinting in stem cells and niche astrocytes regulates neurogenesis. *Nature*, *475*, 381–385.

Fregosi, M., Contestabile, A., Badoud, S., Borgognon, S., Cottet, J., Brunet, J.-F., & Rouiller, E. M.(2019). Corticotectal Projections From the Premotor or Primary Motor Cortex After Cortical Lesion or Parkinsonian Symptoms in Adult Macaque Monkeys: A Pilot Tracing Study. *Frontiers in Neuroanatomy*, *13*, 50.

Frost, S. B., Milliken, G. W., Plautz, E. J., Masterton, R. B., & J. Nudo, R. J. (2000). Somatosensory and motor representations in cerebral cortex of a primitive mammal (*Monodelphis domestica*): A window into the early evolution of sensorimotor cortex. *The Journal of Comparative Neurology*, *421*, 29–51.

Ioannides, Y., Lokulo-Sodipe, K., Mackay, D. J., Davies, J. H., & Temple, I. K. (2014). Temple syndrome: Improving the recognition of an underdiagnosed chromosome 14 imprinting disorder: An analysis of 51 published cases. *Journal of Medical Genetics*, *51*, 495–501.

Irie, M., Yoshikawa, M., Ono, R., Iwafune, H., Furuse, T., Yamada, I., & Kaneko-Ishino, T.(2015). Cognitive Function Related to the *Sirh11/Zcchc16* Gene Acquired from an LTR Retrotransposon in Eutherians. *PLoS Genetics*, *11*, e1005521.

Irie, M., Koga, A., Kaneko-Ishino, T., & Ishino, F. (2016). An LTR Retrotransposon-Derived Gene Displays Lineage-Specific

Structural and Putative Species-Specific Functional Variations in Eutherians. *Frontiers in Chemistry*, *4*, 26.

Iwaniuk, A. N., & Whishaw, I. Q. (2000). On the origin of skilled forelimb movements. *Trends in Neuroscience*, *23*, 372–376.

Ivanco, T. L., Pellis, S. M., & Whishaw, I. Q. (1996). Skilled forelimb movementsin prey catching and in reaching by rats (Rattusnorvegicus) and opossums (Monodelphisdomestica) relations to anatomical differences in motor systems. *Behavioral Brain Research*, *79*, 163–181.

Kagami, M., Nishimura, G., Okuyama, T., Hayashidani, M., Takeuchi, T., Tanaka, S., & Ogata, T.(2005). Segmental and full paternal isodisomy for chromosome 14 in three patients: Narrowing the critical region and implication for the clinical features. *American Journal of Medical Genetics. Part A*, *138A*, 127–132.

Kagami, M., Sekita, Y., Nishimura, G., Irie, M., Kato, F., Okada, M., & Ogata, T.(2008). Deletions and epimutations affecting the human chromosome 14q32.2 imprinted region in individuals with paternal and maternal upd(14)-like phenotypes. *Nature Genetics*, *40*, 237–242.

Kagami, M., Kurosawa, K., Miyazaki, O., Ishino, F., Matsuoka, K., & Ogata, T. (2015). Comprehensive clinical studies in 34 patients with molecularly defined UPD(14)pat and related conditions (Kagami-Ogata syndrome). *European Journal of Human Genetics*, *23*, 1488–1498.

Kagami, M., Nagasaki, K., Kosaki, R., Horikawa, R., Naiki, Y., Saitoh, S., & Ogata, T.(2017). Temple syndrome: Comprehensive molecular and clinical findings in 32 Japanese patients. *Genetics in Medicine*, *19*, 376–482.

Kaneko-Ishino, T., & Ishino, F. (2012). The role of genes domesticated from LTR retrotransposons and retroviruses in mammals. *Frontiers in Microbiology*, *3*, 262.

Kaneko-Ishino, T., & Ishino, F. (2015). Mammalian-specific genomic functions: Newly acquired traits generated by genomic imprinting and LTR retrotransposon- derived genes in mammals. *Proceedings of the Japan Academy Series B Physical and Biological Sciences*, *91*, 511–538.

Keshavarzi, S., Sullivan, R. K. P., Ianno, D. J., & Sah, P. (2014). Functional Properties and Projections of Neurons in the Medial Amygdala. *Journal of Neuroscience*, *34*, 8699–8715.

Kitazawa, M., Tamura, M., Kaneko-Ishino, T., & Ishino, F. (2017). Severe damage to the placental fetal capillary network causes mid to late fetal lethality and reduction of placental size in *Peg11/Rtl1* KO mice. *Genes to Cells*, *22*, 174–188.

Kitazawa, M., Hayashi, S., Imamura, H., Takeda, S., Oishi, Y., Kaneko-Ishino, T., & Ishino, F. (2020). Deficiency and overexpression of *Rtl1* in the mouse cause distinct muscle abnormalities related to the Temple and Kagami-Ogata syndromes. *Development*, *147*, dev185918.

Kotzot, D. (2004). Maternal uniparental disomy 14 dissection of the phenotype with respect to rare autosomal recessively inherited traits, trisomy mosaicism, and genomic imprinting. *Annales De Genetique*, *47*, 251–260.

Lavialle, C., Cornelis, G., Dupressoir, A., Esnault, C., Heidmann, O., Vernochet, C., & Heidmann, T. (2013). Paleovirology of "syncytins", retroviral env genes exapted for a role in placentation. *Philosophical Transactions of the Royal Society of London. Series B, Biological Sciences*, *368*, 20120507.

Lemon, R. N. (2008). Descending Pathways in Motor Control. *Annual Review of Neuroscience*, *31*, 195–218.

Mi, S., Lee, X., Li, X., Veldman, G. M., Finnerty, H., Racie, L., & McCoy, J. M.(2000). Syncytin is a captive retroviral envelope protein involved in human placental morphogenesis. *Nature*, *403*, 785–789.

Mihrshahi, R. (2006). The corpus callosum as an evolutionary innovation. *Journal of Experimental Zoology*, *306B*, 8–17.

Moon, Y. S., Smas, C. M., Lee, K., Villena, J. A., Kim, K.-H., Yun, E. J., & Sul, H. S. (2002). Mice lacking paternally expressed Pref-1/dlk1 display growth retardation and accelerated adiposity. *Molecular and Cellular Biology*, *22*, 5585–5592.

Nakaya, Y., Koshi, K., Nakagawa, S., Hashizume, K., & Miyazawa, T. (2013). *Fematrin-1* is involved in fetomaternal cell-to-cell fusion in Bovinae placenta and has contributed to diversity of ruminant placentation. *Journal of Virology*, *87*, 10563–10572.

Naruse, M., Ono, R., Irie, M., Nakamura, K., Furuse, T., Hino, T., & Kaneko-Ishino, T.(2014). *Sirh7/Ldoc1* knockout mice exhibit placental P4 overproduction and delayed parturition. *Development*, *141*, 4763–4771.

Ogata, T., & Kagami, M. (2016). Kagami-Ogata syndrome: 687 a clinically recognizable upd(14)pat and related disorder affecting the chromosome 14q32.2 imprinted region. *Journal of Human Genetics*, *61*, 87–94.

Ono, R., Kobayashi, S., Wagatsuma, H., Aisaka, K., Kohda, T., Kaneko-Ishino, T., & Ishino, F. (2001). A retrotransposon-derived gene, *PEG10*, is a novel imprinted gene located on human chromosome 7q21. *Genomics*, *73*, 232–237.

Ono, R., Nakamura, K., Inoue, K., Naruse, M., Usami, T., Wakisaka-Saito, N., & Ishino, F.(2006). Deletion of *Peg10*, an imprinted gene acquired from a retrotransposon, causes early embryonic lethality. *Nature Genetics*, *38*, 101–106.

Pastuzyn, E. D., Day, C. E., Kearns, R. B., Kyrke-Smith, M., Taibi, A. V., McCormick, J., & Shepherd, J. D. (2018). The Neuronal Gene *Arc* Encodes a Repurposed Retrotransposon Gag Protein that Mediates Intercellular RNA Transfer. *Cell*, *172*, 275–288.

Patestas, M., & Gartner, L. P. (2019). A Textbook of Neuroanatomy, Second Edition. Wiley Blackwell, pp 228-249 and 479-565, (2016).

Pardo-Bellver, C., Cádiz-Moretti, B., Novejarque, A., Martínez-García, F., & Lanuza, E. (2012). Differential efferent projections of the anterior, posteroventral, and posterodorsal subdivisions of the medial amygdala in mice. *Frontiers in Neuroanatomy*, *6*, 33.

Perreault, M.-C., & Giorgi, A. (2019). Diversity of reticulospinal systems in mammals. *Current Opinion in Physiology*, *8*, 161–169.

Sekita, Y., Wagatsuma, H., Nakamura, K., Ono, R., Kagami, M., Wakisaka-Saito, N., & Ishino, F.(2008). Role of retrotransposon-derived imprinted gene, *Rtl1*, in the feto-maternal interface of mouse placenta. *Nature Genetics*, *40*, 243–248.

Suárez, R. I., Gobius, I., & Richards, L. J. (2014). Evolution and development of interhemispheric connections in the vertebrate forebrain. *Frontiers in Human Neuroscience*, *8*, 497.

Warburton, E. C., Baird, A. L., Morgan, A., Muir, J. L., & Aggleton, J. P. (2000). Disconnecting hippocampal projections to the anterior thalamus produces deficits on tests of spatial memory in rats. *European Journal of Neuroscience*, *12*, 1714–1726.

Yevtodiyenko, A., & Schmidt, J. V. (2006). Dlk1 expression marks developing endothelium and sites of branching morphogenesis in the mouse embryo and placenta. *Developmental Dynamics*, *235*, 1115–1123.

Zhang, C.-L., Houbaert, X., Lepleux, M., Deshors, M., Normand, E., Gambino, F., & Humeau, Y.(2015). The hippocampo-amygdala

control of contextual fear expression is affected in a model of intellectual disability. *Brain Structure and Function*, *220*, 3673–3682.

SUPPORTING INFORMATION

Additional supporting information may be found online in the Supporting Information section.

How to cite this article: Kitazawa M, Sutani A, Kaneko-Ishino T, Ishino F. The role of eutherian-specific *RTL1* in the nervous system and its implications for the Kagami-Ogata and Temple syndromes. *Genes Cells*. 2021;26:165–179. https://doi.org/10.1111/gtc.12830